AUT Journal of Electrical Engineering

AUT J. Elec. Eng., 51(1) (2019) 45-54
DOI: 10.22060/eej.2018.14172.5210

A Novel Hybrid-Excited Modular Variable Reluctance Motor for Electric Vehicle Applications: Analysis, Comparison, and Implementation

M. A. Jalali Kondelaji[1,2], M. Mirsalim[1,2]

ABSTRACT: A variable reluctance machine (VRM) has been proven to be an outstanding candidate for electric vehicle (EV) applications. This paper introduces a new double-stator, 12/14/12-pole three-phase hybrid-excited modular variable reluctance machine (MVRM) for EV applications. In order to demonstrate the superiorities of the proposed structure, the static torque characteristics and dynamic performances of the novel MVRM are compared with the other two VRMs with similar dimensions and parameters. Then, the steady-state performance of the proposed motor with single-pulse control (SPC) for two operating speeds is obtained. Additionally, the cogging torque profile of the machine is derived. Finally, the motor performance is investigated under faulty conditions. The proposed MVRM is built and the test results are obtained. Both of the simulation and test results indicate that the proposed MVRM produces a higher average torque compared to the other two machines in the same operational speeds, with an ignorable cogging torque.

Review History:
Received: 6 March 2018
Revised: 20 November 2018
Accepted: 31 December 2018
Available Online:31 December 2018

Keywords:
Electric vehicle applications
hybrid-excited machine
single-pulse control (SPC)
variable reluctance machine

1- Introduction

With the advent of the electric vehicle industry, selecting an appropriate alternative for use in electric vehicle (EV) applications has become a challenging issue in the field of electric machines. Variable reluctance machines (VRMs) have been shown to be suitable candidates for numerous applications such as safety-critical applications and electric vehicles [1-3]. This is because of their distinguished merits such as rigid and robust structure, low construction cost, no permanent magnets or windings on the rotor, simple cooling, inherent fault-tolerance, and high-speed capability. However, VRMs are still suffering from some disadvantages, including lower torque and power densities and higher torque ripple compared to other machines.

Recently, many researchers have reported on different methods to improve the characteristics of VRMs to make them more popular to industry applications. These methods include optimization of classical rotors and stators [4-6] and offering novel control methods [7, 8].

Among the broad variety of VRM structures, modular variable reluctance motors (MVRMs) exhibit more advantages than the other forms. In MVRMs, owing to a sufficient spacing between the adjacent phases, the mutual coupling, which is a complex feature for machine analysis can be ignored. Moreover, in MVRMs there is a significant steel saving, which accordingly leads to less iron loss, higher efficiency, and lower manufacturing cost. Recent studies have shown that permanent magnets can noticeably enhance the output characteristics of the VRMs with no detrimental impact on the machine reliability. Some methods have been proposed in the literature such as mounting the PMs in the stator back-iron, pole-tips, or pole-to-pole area [9-13], all of which prove the remarkable capability of the method. Also, in [14], four hybrid-excitation variable reluctance machines with C-core stator are thoroughly compared.

Another method to improve the shortcomings of the VRMs is to employ the modular double-stator structures, which enhances the average torque, flux density, and output power while mitigating the flux leakage and iron losses.

The main contribution of this paper is presenting a novel hybrid-excited double-stator variable reluctance machine with modular structures and a higher number of the rotor poles than the stator poles. This work was preliminarily presented in [15] inspired by the work of Andrada about hybrid-excited reluctance motors [11]. This paper is organized as follows. Section 2 introduces a novel proposed structure and its static performance. Then, in section 3, the static and dynamic performances of the machine and other two VRMs are obtained and compared through a 2-D finite-element analysis to better clarify the superior operation of the proposed MVRM. The normal dynamic performance of the MVRM with single-pulse control (SPC) is given in section 4. Also, section 4 investigates the faulty performance of the proposed MVRM. In section 5, the prototype motor is built and the experimental results are provided. Finally, a concise conclusion is given in section 6.

2- Machine structure and static analysis

The cross-section view of the proposed MVRM is presented in Fig. 1(a). This MVRM comprises two stators: an inner 12-pole conventional stator, an outer stator with six magnetically-disconnected diametrically-placed C-shaped modules, and a

Corresponding author, E-mail:

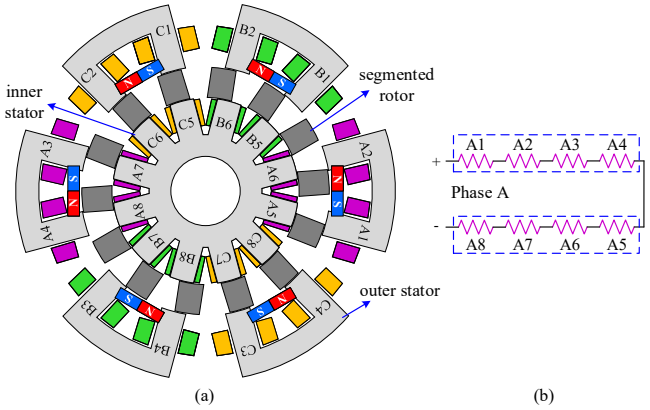

Fig. 1. (a) Cross-section view of the proposed MVRM, (b) arrangement of eight coils in one phase

rotor with fourteen segments, indicating that this machine has a higher number of rotor poles than the stator poles. There are three phases that each one consists of eight windings wound on the teeth of the inner and outer stators and then connected in series, as shown in Fig. 1(b). In addition, six permanent magnets are placed in the pole-to-pole area, connecting the outer modules teeth to form six closed C-core electromagnets. The operating principle of the proposed MVRM is elucidated in Fig. 2. When only the coil is excited (Fig. 2(a)), the flux track is closed through the air-gaps. If there is no current in the winding, the flux of the PM closes itself through the back-iron of the C-core (Fig. 2(b)). Now, when the coil is also excited, the flux path of the PM adds to that of the module generated by the excited coil (Fig. 2(c)) and hence, the attraction force enhances, which results in a significant increase in the output torque of the motor.

One of the notable features of the proposed MVRM is the form of its aligned position. In contrast to other machines, in which the rotor and stator poles are aligned symmetrically, in this novel machine the aligned position is different to some extent, which will be discussed in section three meticulously. The main geometric dimensions and parameters of the machine are tabulated in Table 1. In order to achieve the static performance of the proposed machine, a 2-D finite-element analysis is employed. Figure 3(a) shows the static torque curves as a function of the rotor position for different currents when only one phase of the machine is energized. The torque curves are obtained for a 180°_{elec} (10.71°_{mech}) conduction interval. In addition, the meshed model of the structure is illustrated in Fig. 3(b).

One detrimental effect which originates from the higher ranges of the excitation current is the irreversible demagnetization of the PM material. Figure 4 shows the magnetic flux density

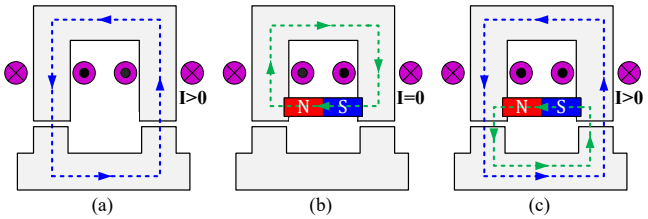

Fig. 2. Flux path of (a) the module with only coil excitation, (b) the PM without current in the coil, and (c) the PM and the coil with a current in the coil

Table 1. Geometric dimensions and key parameters of the proposed MVRM.

Parameter	Value	Parameter	Value
Number of poles	12/14/12	Outer stator yoke diameter	6.9mm
Outer stator inner/ outer diameter	114/74.8 mm	Inner stator yoke width	6.3mm
Inner stator diameter	55.6 mm	Rotor pole width	7.4mm
Outer/inner stator pole arcs	11.47°/15°	Number of turns per outer/inner stator pole	72/20
Rotor outer/inner pole arcs	15.1°/11.37°	PM thickness	3.5mm
Air-gap length	0.3 mm	PM material	NdFeB35
Stack length	53 mm	Electric steel material	M19-24G

distributions of the machine at the unaligned position for the excitation current of 25A. As can be observed, the flux density of the PMs is in the range of 0.5-1.3T, which is much larger than 0.4T. Since the phase current in normal operation is lower than 25A, there will be no irreversible demagnetization in the PMs.

In order to consider the 3-D effect, a 3-D FEA is adopted.

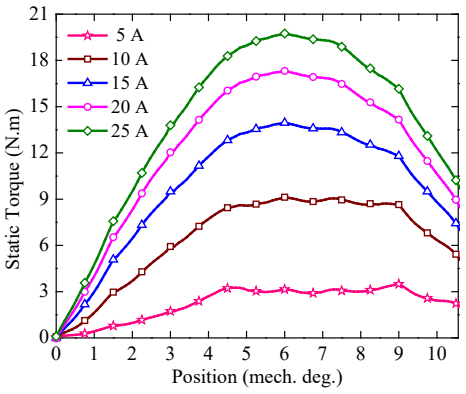

(a)

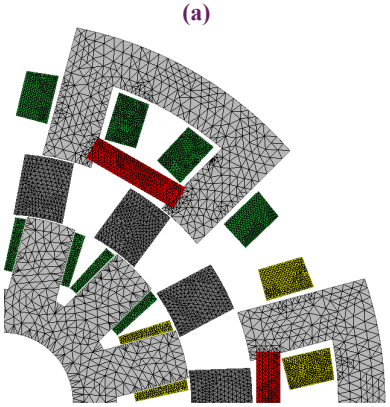

(b)

Fig. 3. (a) Static torque curves for different current values, (b) The meshed model of the structure

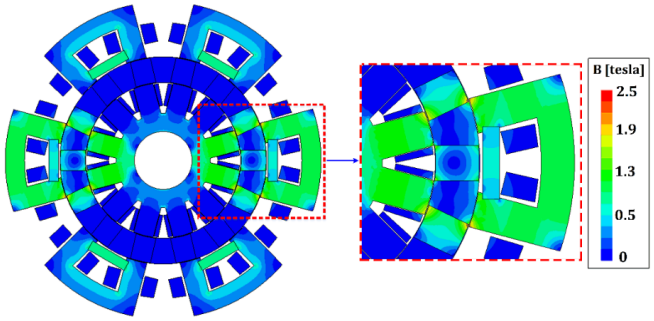

Fig. 4. Magnetic flux density distribution of the machine at the aligned position with the phase current of 25A

The magnetic flux density vectors for the unaligned and aligned positions at the phase current of 10A are depicted in Fig. 5(a). It can be observed that there is no flux reversal in the proposed modular VRM and the magnetic flux travels a very short path. The static torque curves of the introduced MVRM are obtained based on the 3-D FEA for five different currents, as shown in Fig. 5(b). It can be seen that there is a discrepancy between the torque values at different rotor positions. This discrepancy is acceptable and shows the 3-D effect in the design process. It is worthy to note that the 3-D FEA is very time-consuming, hence the 2-D FEA is used to obtain the dynamic results of the proposed motor.

3- Comparison with other VRMs

In order to demonstrate the superior operation of the proposed MVRM, a thorough comparative study is done. Figure 6 shows the cross-section of two other MVRMs; one is the same proposed MVRM without PMs, and the other is a classical 12/14-pole MVRM. In order to have an accurate comparison, all parameters of the three machines, including the number of turns per phase, main dimensions, DC-link

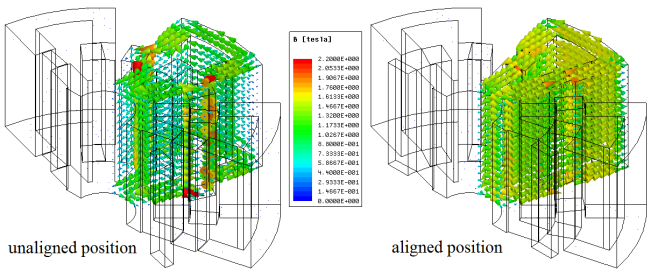

(a)

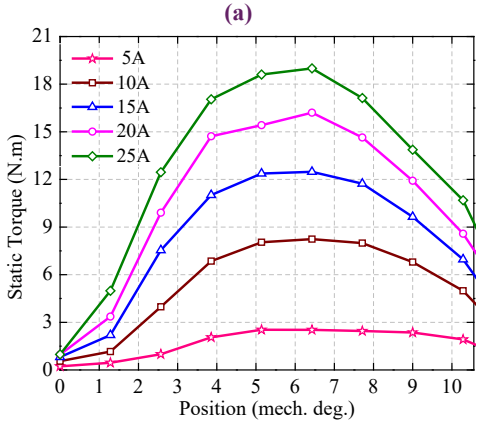

(b)

Fig. 5. The 3-D FEA results of the proposed motor. (a) Magnetic flux density vectors. (b) Static torque profiles

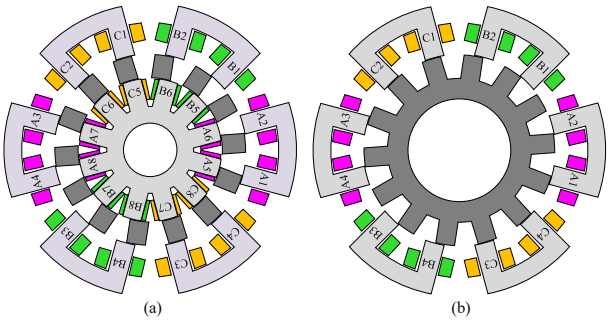

(a) (b)

Fig. 6. Cross-section view of (a) the proposed MVRM without PMs and (b) the conventional MVRM

voltage, turn-on and turn-off angles, and the nominal speed are assumed to be the same.

In order to analyze the operation of the three machines, the flux lines are depicted in Fig. 7. It can be understood from Fig. 7(a) that when the windings are energized, the flux generated by the permanent magnets crosses the air-gaps, and adds to the flux density of the air-gaps. Hence, the output torque increases. The flux paths in the novel MVRM without PMs and the classical MVRM are plotted in Figs. 7(b) and (c), respectively for both the aligned and unaligned positions.

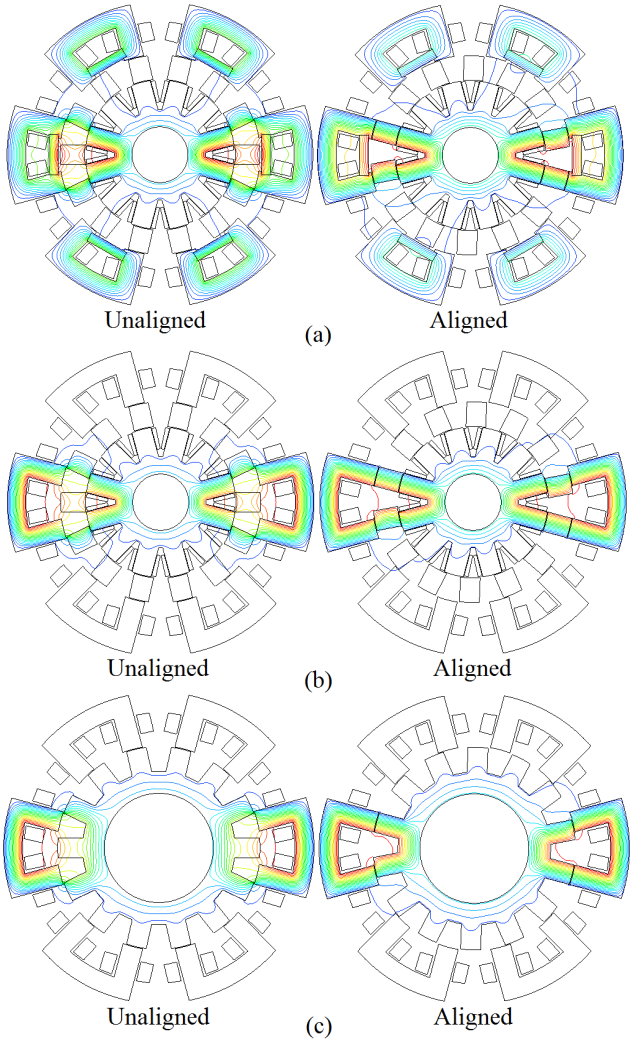

Fig. 7. Flux distribution of the three motors at the unaligned and aligned positions. (a) The PM-assisted MVRM, (b) MVRM without PMs, and (c) the conventional MVRM

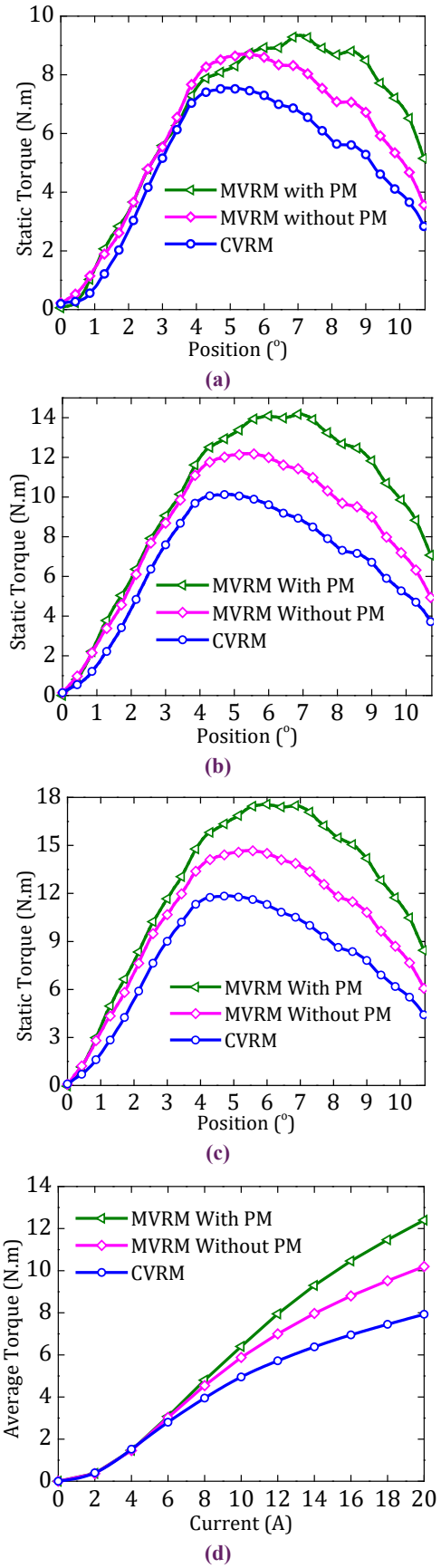

Fig. 8. Comparative curves of the static torque at (a) 10A, (b) 15A, (c) 20A, and (d) average torque for different current values

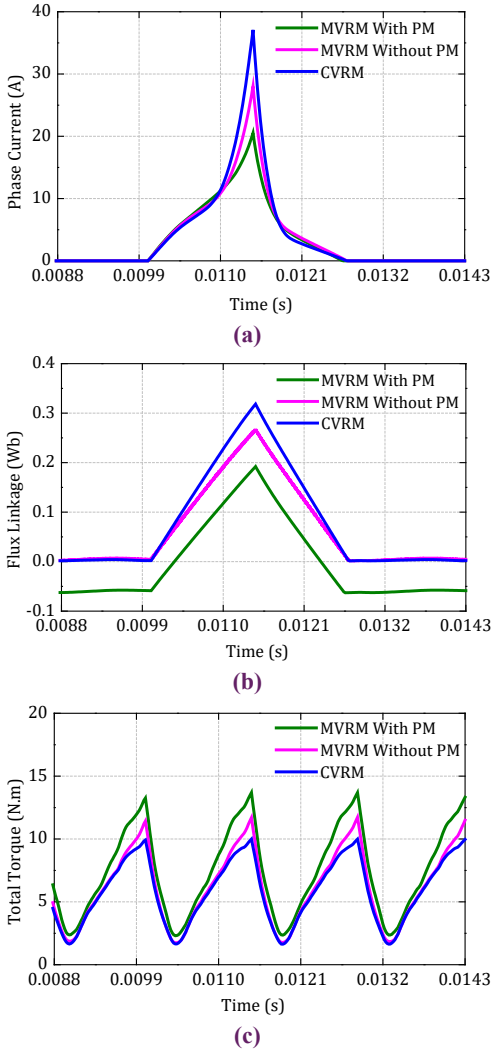

Fig. 9. Comparative curves of dynamic performance with SPC. (a) Phase current, (b) flux linkage, and (c) total torque at 1000rpm.

As noted before, despite the classical topologies, the aligned position is different here. In classical VRMS, when the rotor starts from the unaligned position, the output torque increases to a specific value and then decreases until it gets to zero, which means that the rotor has reached to its fully aligned position. This statement indicates that the center line of the stator tooth is aligned to that of the rotor, i.e., the deflection angle is zero. In the proposed model, the deflection angle, which has a significant effect on the air-gap reluctance, is not zero. This angle leads to a lower torque ripple.

In order to illustrate the superior performance of the novel MVRM, the static and dynamic results for the three MVRMs are carried out. In Figures 8(a), (8b), and (8c), the comparative curves of the static torque versus the rotor position are plotted for three different currents when only one phase is excited. The static analysis shows that when the current in the coils increases, the difference between the hybrid-excited and the other two MVRMs becomes more significant. The average static torque of single-phase excitation for different current values is also given in Fig. 8(d). Figure 9 illustrates the comparative dynamic results. In this study, the DC-link voltage is fixed at 180V with single-pulse control (SPC) mode with the nominal speed of 1000 rpm. The turn-on and

turn-off angles are 0° and 8.57°, respectively. The number of turns-per-pole for the conventional motor is 92 and the number of turns-per-pole for the inner and outer stator of the new topology with and without PMs are taken as 20 and 72, respectively. Hence, the copper volume is the same in the three compared machines. Figure 9(a) shows that the maximum phase current of the conventional MVRM is much higher than that of the proposed MVRMs (with and without PMs). However, it produces a lower torque compared to the novel proposed structures, which is shown in Fig. 9(b). Also, there is a great difference between the two MVRMs with and without PMs, in a way that the hybrid-excited structure produces a higher torque with a lower phase current. Figure 9(c) presents the flux linkage of the three machines.

Another comparison is done with the HRM proposed in [11]. Based on this reference, the work of Andrada is a three-phase 6/5 HRM. The main difference between our proposed structure and the structure in [11] is the superiority of the proposed MVRM in terms of the symmetry of the radial forces. Fig. 10 depicts the graph of the radial forces and the deformation of the stator caused by the radial forces. Figs. 10(a) and 10(b) illustrate the deformation of the stator of the HRM proposed in [11] and the proposed MVRM, respectively. This figure vividly demonstrates that the radial forces of the proposed MVRM are symmetric. And hence, the deformation of the stator does not damage the stator structure, while the radial forces of the HRM in [11] is asymmetric, which deforms the shape of the stator.

Moreover, the proposed MVRM is composed of six modules offering a higher winding space. Also, the proposed MVRM is a dual-stator machine, and the unnecessary space for the rotor is being utilized as an inner stator. Based on these properties, the proposed MVRM produces a higher torque than the HRM in [11].

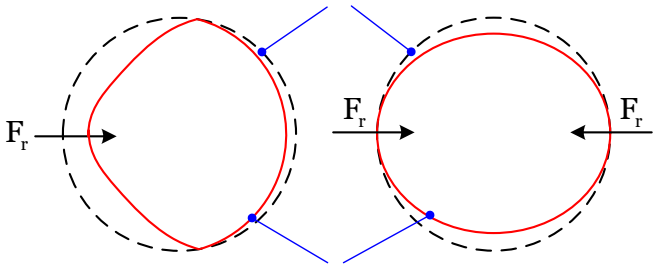

Fig. 10. Radial forces and deformation of the stator caused by radial forces. (a) HRM in [10]. (b) Proposed MVRM

4- Dynamic Analysis

4- 1- Normal Dynamic Performance

A comprehensive dynamic analysis of the machine is provided with an SPC mode at two different operating speeds. The turn-on and turn-off angles are taken 0° and 8.57°, respectively. The DC-link voltage is 110V. Figure 11 illustrates the dynamic waveforms at the speed of 1000rpm, which proves the aforementioned statements, i.e., the output torque has increased because of the increase in the phase current. In this condition, the mean torque is 3.76 Nm, where the RMS value of the current is 4.9A. Meanwhile, the torque ripple is 143%. The phase current waves and the total torque

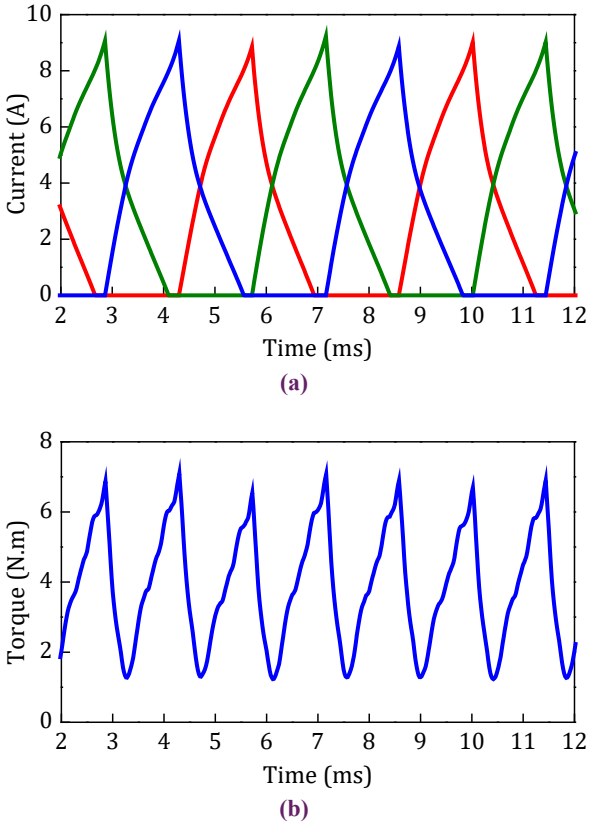

Fig. 11. Dynamic waveforms of the proposed MVRM. (a) The current of the phases and (b) total torque at 1000rpm with SPC

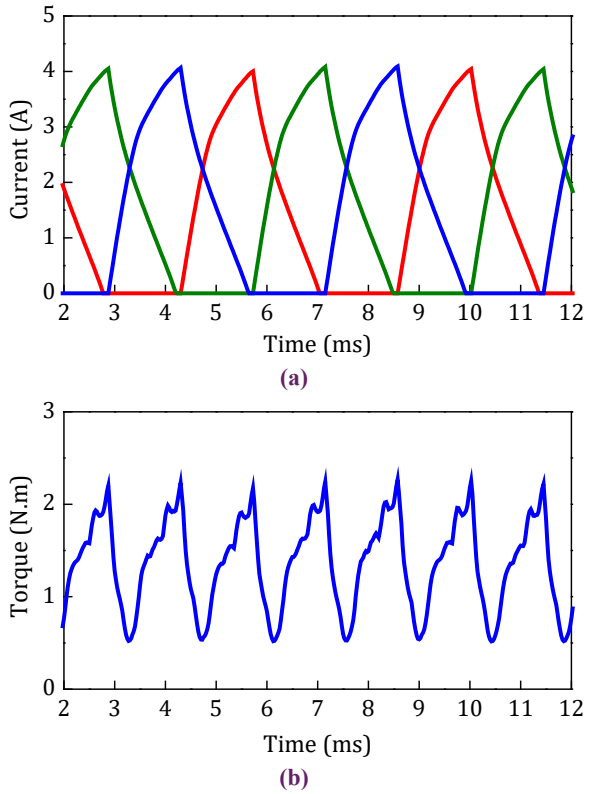

Fig. 12. Dynamic waveforms of the proposed MVRM. (a) The current of the phases and (b) total torque at 1500rpm with SPC.

at the speed of 1500rpm are shown in Fig. 12. The mean torque in this condition is 1.57 Nm, and the torque ripple is 109%. As the operating speed decreases, the RMS value of the phase current increases which results in a higher output torque.

A summary of the steady-state characteristics of the three machines is listed in Table 2. It can be deduced that when the operating speed is low, the proposed MVRM has a higher average torque than the other two VRMs. However, due to the current chopping control (CCC) mode at low speeds, the RMS phase currents of the three machines are the same. In addition, the MVRM presents a higher average torque than the two VRMs at the speed of 1000rpm, while it has the lowest RMS phase current among the three machines. In other words, with the proposed topology, higher torques are obtained with lower currents. Among these three motors, the MVRM presents the lowest torque ripple in the whole speed range.

Table 2. Comparison of the steady-state operation of the three machines

	MVRM with PM		MVRM without PM		CVRM	
Control mode	CCC	SPC	CCC	SPC	CCC	SPC
Speed, rpm	400	1000	400	1000	400	1000
DC bus voltage, V	150	190	150	190	150	190
RMS phase current, A	7.54	5.57	7.49	5.97	7.65	6.11
Average torque, Nm	7.29	4.79	6.45	4.31	5.96	3.89
Torque ripple, %	124	137	139	161	143	153
Copper Loss, W	119.4	65.1	117.8	74.8	105.3	67.2
Output power, W	305.4	501.6	270.2	451.3	249.7	407.4
Power per copper loss, W/W	2.557	7.705	2.293	6.033	2.371	6.062
Torque per ampere, Nm/A	0.966	0.856	0.872	0.742	0.769	0.636
Power per ampere, W/A	40.51	90.05	36.07	75.59	32.64	66.67

4- 2- Start-up Operation

The transient operation of the proposed MVRM is obtained using FEA, as shown in Fig. 13. In this case, the DC-link voltage is set to 190V. The load torque is 1.5Nm and the turn-on and turn-off angles are fixed at 0° and 120° electrical degrees, respectively. It has to be mentioned that during the start-up the motor is operated with the CCC mode, in which the reference and bandwidth currents are 15.5A and 1A, respectively. It can be observed that the settling time of the proposed MVRM is about 0.05s and the steady-state speed of the motor is 1194rpm. In addition, this motor can successfully perform self-starting. Finally, the torque-speed and power-speed characteristics of the proposed structure and the other two motors are obtained, as shown in Fig. 14. In this study, the DC-link voltage is fixed at 190V and controlled with the CCC mode (with the reference current of 15.5A) for low-speed operations and SPC mode at high-speed operations.

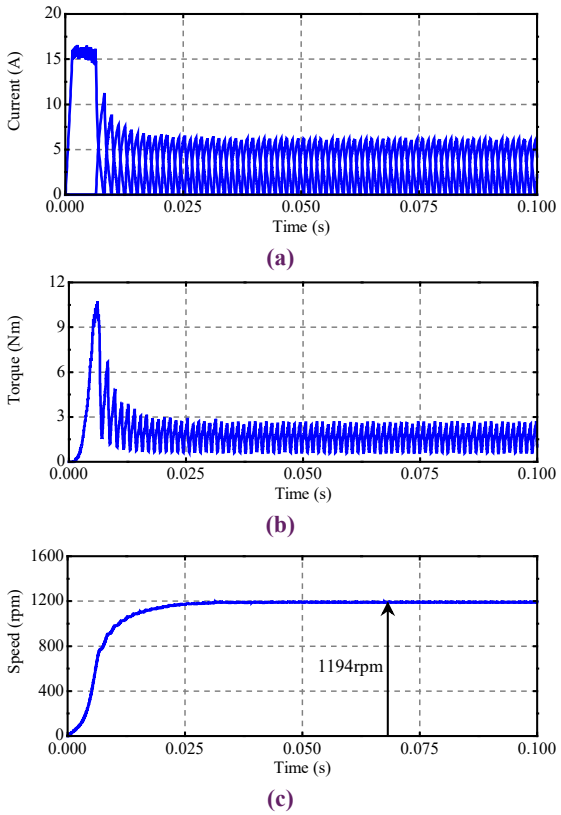

Fig. 13. Transient waveforms for start-up operation of the MVRM. (a) Current. (b) Torque. (c) Speed

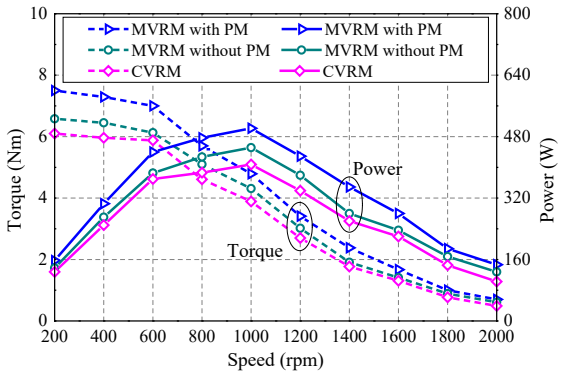

Fig. 14. Torque and power versus speed characteristics of the three MVRMs

The simulation results indicate that the proposed MVRM has a higher torque and power than the other two machines in the whole speed range. The rated speed and rated power of the new machine are 1000rpm, and 500W, respectively.

4- 3- Cogging torque analysis

When the coils are excited, in the presence of the PMs, the machine operates in a normal condition. When there is no current in the windings, torque exists because of the presence of the PMs. This torque, which has a detrimental impact on the machine operation, is called cogging torque. In order to obtain the cogging torque of the structure, which is also called detent torque, none of the coils are energized. The cogging torque profile of the proposed structure is illustrated in Fig. 15. It can be noted that the cogging torque of the machine is around zero (between -3 and 3 mN.m). Hence, when only one

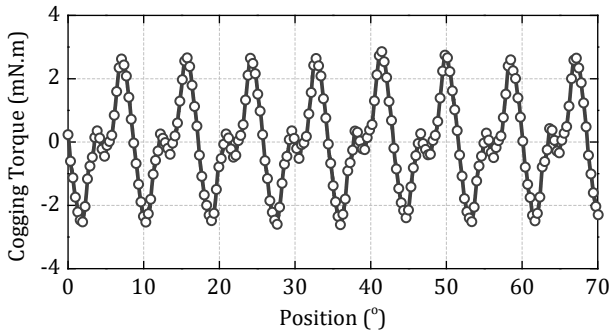

Fig. 15. Cogging torque of the proposed MVRM

phase conducts and the other two phases only experience the presence of the PMs, there is no disturbance in the machine performance. This is one of the other superiorities of this type of machine.

4- 4- Faulty performance

One momentous issue in most safety-critical applications, especially EV applications is the fault-tolerance capability. The novel MVRM inherently provides a satisfactory fault-tolerance capability. Figure 16 shows the faulty waveforms of the machine. In this study, the DC-link voltage is fixed at 110V. The nominal speed is 1000rpm. Phase 'B' of the machine is assumed to be faulted. As Fig. 16(a) shows, the current flow through the coils of phase B is zero. The output torque is plotted in Fig. 16(b). In this faulty condition, the average torque is 2.52 N.m. (which was 3.76 N.m. during the normal operation), which means that the machine still has a satisfactory operation. This plainly indicates the outstanding fault- tolerance capability of the proposed structure.

4- 5- Back-EMF and induced voltage analysis

In order to obtain the back-EMF waveforms of the proposed

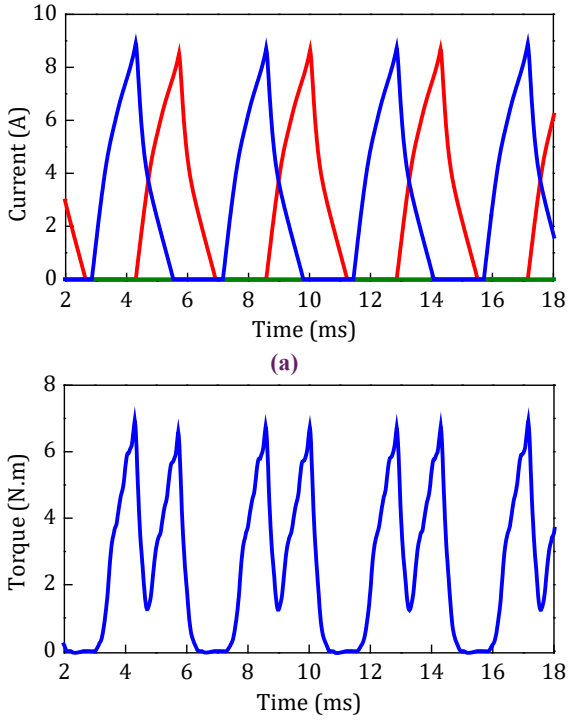

Fig. 16. Faulty performance waveforms. (a) Current and (b) total torque at 1000rpm with the SPC

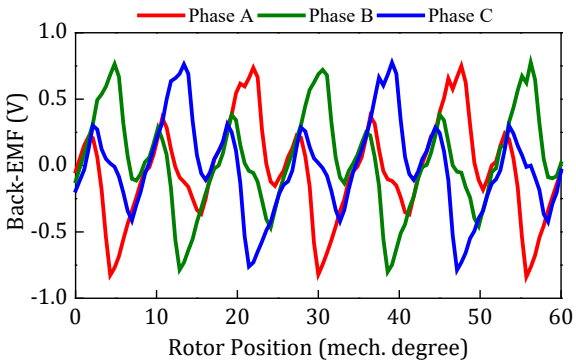

Fig. 17. Back-EMF waveforms of the proposed PM-assisted MVRM at 1000 rpm

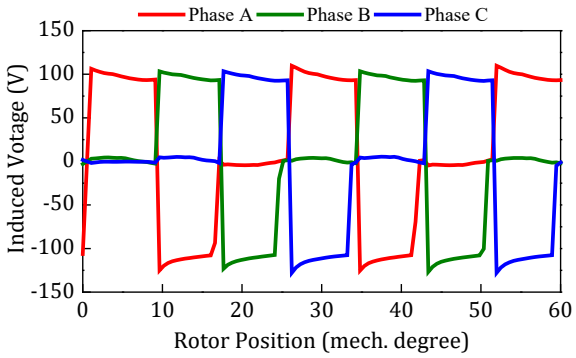

Fig. 18. Induced voltage waveforms of the proposed PM-assisted MVRM at 1000rpm

motor, the excitation current of the phases should be fixed at zero. Fig. 17 shows the back-EMF results at a speed of 1000rpm. It has to be mentioned that the concept of back-EMF is not usual in variable reluctance motors since the principle of operation is based on the reluctance variations. Accordingly, we do not expect a sinusoidal waveform for back-EMF, which is in a different category compared to the PMSMs or FSPMs. Additionally, as can be seen from Fig. 17, the amplitude of the back-EMF waveform is small, in contrast to the PMSMs or FSPMs. Also, the back-EMF waveforms do not have any contributions in the operation of the VRMs.

The induced voltage waveforms in the steady-state operation of the proposed PM-assisted MVRM at the nominal speed of 1000rpm are depicted in Fig. 18. In order to obtain these characteristics, the proposed motor is linked to the external circuit (Asymmetric full-bridge inverter) and the SPC (single pulse control) strategy is employed with the input DC voltage of 110V. When the gates of the MOSFETs in one leg of the inverter are pulsed at turn-on angle of 0° ($\theta_{on} = 0^{\circ elec}$), the induced voltage in the phase is about 110V. When the MOSFETs are turned off at 120 electrical degree ($\theta_{off} = 120^{\circ elec}$), the induced voltage in the phase becomes negative, since there is still current in the windings. When the current of the phase becomes zero, the induced voltage in the phase becomes zero, too.

5- Experimental results

In order to validate the simulation results, a prototype motor is built. Fig. 19(a) shows the structure of the inner and outer stators. The outer stator is composed of six independent modules and the inner stator has a conventional structure.

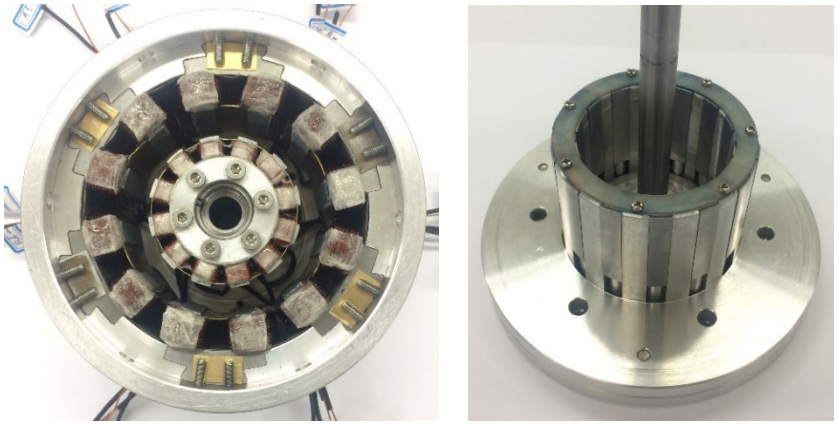

(a) (b)

Fig. 19. A prototype of the proposed MVRM. (a) Inner and outer stators. (b) Rotor structure

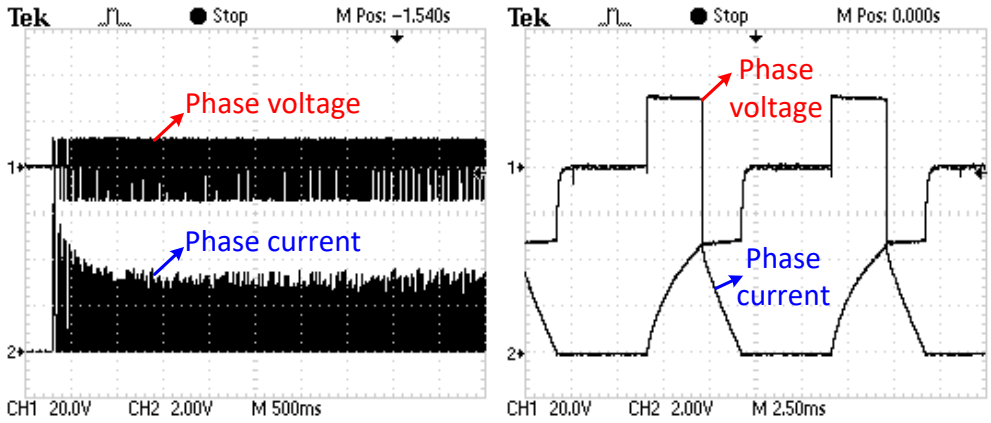

(a) (b)

Fig. 20. Measured voltage and current waveforms in (a) large-time division, (b) small-time division

Fig. 19(b) shows the structure of the rotor with fourteen independent segments.

Fig. 20 shows the measured voltage and current waveforms. In Fig. 20(a), the current waveforms at the start-up operation of the motor are depicted. In order to better clarify the waveforms, Fig. 20(b) is provided in a small-time division. The results are compatible with those obtained from the FEA.

6- Conclusion

This paper presented an innovative double-stator hybrid-excited 12/14/12-pole modular variable reluctance machine with a segmental rotor. The machine static torque curves were obtained through 2-D and 3-D finite-element analyses. In order to show the superior performance of the machine, the dynamic and static results of the proposed model and the other two machines were obtained and compared. This comparative study demonstrated the outperformance of the proposed MVRM over the other two machines. The normal dynamic performance of the proposed machine was also obtained for different operating speeds. Also, the cogging torque profile was obtained and it was shown that this torque approximated to zero, and therefore could be overlooked. Finally, the performance of the MVRM under a faulty condition was investigated. It was illustrated that the proposed topology operated satisfactorily in the faulty conditions, which showed the capability of the proposed machine as a viable candidate for EV applications. Finally, the proposed MVRM was constructed and the experimental results were given to validate the simulation results.

References

[1] M. Ruba, I.-A. Viorel, L. Szabó, Modular stator switched reluctance motor for fault tolerant drive systems, *IET Electr. Power Appl.*, 7(3) (2013) 159-169.

[2] A. Labak, N.C. Kar, Designing and prototyping a novel five-phase pancake-shaped axial-flux SRM for electric vehicle application through dynamic FEA incorporating flux-tube modeling, *IEEE Transactions on Industry Applications*, 49(3) (2013) 1276-1288.

[3] W. Ding, Y. Hu, L. Wu, Analysis and development of novel three-phase hybrid magnetic paths switched reluctance motors using modular and segmental structures for EV applications, *IEEE/ASME Transactions on Mechatronics*, 20(5) (2015) 2437-2451.

[4] G. Li, J. Ojeda, S. Hlioui, E. Hoang, M. Lecrivain, M. Gabsi, Modification in rotor pole geometry of mutually coupled switched reluctance machine for torque ripple mitigating, *IEEE Transactions on Magnetics*, 48(6) (2011) 2025-2034.

[5] H. Eskandari, M. Mirsalim, An improved 9/12 two-phase E-core switched reluctance machine, *IEEE Trans. Energy Convers.*, 28(4) (2013) 951-958.

[6] M.A.J. Kondelaji, S.A. Ansari, M. Mirsalim, J.S.

Moghani, Modeling and Analysis of a Modular Switched Reluctance Motor for EV Applications, *Electrical machines letters*, 1(1) (2018).

[7] X. Xue, K. Cheng, S. Ho, Optimization and evaluation of torque-sharing functions for torque ripple minimization in switched reluctance motor drives, *IEEE transactions on power electronics,* 24(9) (2009) 2076-2090.

[8] D.-H. Lee, J. Liang, Z.-G. Lee, J.-W. Ahn, A simple nonlinear logical torque sharing function for low-torque ripple SR drive, *IEEE Transactions on Industrial Electronics*, 56(8) (2009) 3021-3028.

[9] K. Chau, J. Jiang, Y. Wang, A novel stator doubly fed doubly salient permanent magnet brushless machine, *IEEE Transactions on Magnetics*, 39(5) (2003) 3001-3003.

[10] W.-H. Tai, M.-C. Tsai, Z.-L. Gaing, P.-W. Huang, Y.-S. Hsu, Novel stator design of double salient permanent magnet motor, *IEEE Trans. Magn.*, 50(4) (2014) 1-4.

[11] P. Andrada, B. Blanque, E. Martinez, M. Torrent, A novel type of hybrid reluctance motor drive, *IEEE Trans. Ind. Electron.*, 61(8) (2014) 4337-4345.

[12] M. Masoumi, M. Mirsalim, E-core hybrid reluctance motor with permanent magnets inside stator common poles, *IEEE Transactions on Energy Conversion*, 33(2) (2017) 826-833.

[13] M. Masoumi, M.A.J. Kondelaji, M. Mirsalim, J.S. Moghani, Analytical modelling and experimental verification of E-type reluctance motors, *IET Electric Power Applications*, 13(1) (2018) 110-118.

[14] M. Masoumi, M. Mirsalim, A comprehensive comparison between four different C-core hybrid reluctance motors, in: 2017 8th Power Electronics, Drive Systems & Technologies Conference (PEDSTC), *IEEE*, (2017) 114-118.

[15] M.A.J. Kondelaji, M. Mirsalim, Double-stator PM-assisted modular variable reluctance motor for EV applications, in: Power Electronics, Drives Systems and Technologies Conference (PEDSTC), 2018 9th Annual, *IEEE*, (2018) 236-240.

Please cite this article using:

M. A. Jalali Kondelaji, M. Mirsalim, A Novel Hybrid-Excited Modular Variable Reluctance Motor for Electric Vehicle Applications: Analysis, Comparison, and Implementation, *AUT J. Elec. Eng.*, 51(1) (2019) 45-54.

DOI: 10.22060/eej.2018.14172.5210